Materials Transactions, Vol. 46, No. 5 (2005) pp. 996 to 1003

Effect of Chemical Composition on the Optical Properties and Fracture Toughness of Transparent Magnesium Aluminate Spinel Ceramics

Arcan F. Dericioglu[1,*1], Aldo R. Boccaccini[2], Ivo Dlouhy[3] and Yutaka Kagawa[1,*2]

[1]*Institute of Industrial Science, The University of Tokyo, Tokyo 153-8505, Japan*
[2]*Department of Materials, Imperial College London, London SW7 2BP, UK*
[3]*Institute of Physics of Materials, Academy of Sciences of the Czech Republic, Brno 61662, Czech Republic*

Polycrystalline transparent magnesium aluminate "spinel" ceramics were fabricated by hot-pressing and hot isostatic pressing (HIPing) using commercially available MgO and Al_2O_3 powders. Al_2O_3 content of spinel was systematically changed that can be expressed as $MgO{\cdot}nAl_2O_3$ with $n = 1.0$, 1.5 and 2.0. UV/visible and near-IR wavelength region light reflection and transmission behaviors of the spinel ceramics were quantitatively correlated to their microstructure to account for the optical quality of the fabricated materials. The stoichiometric spinel ceramic with $n = 1.0$ revealed a relatively poor optical transparency due to pronounced light scattering at the microcracked grain boundaries with a specular light transmission of ~20–40% in the visible wavelength range. On the other hand, Al_2O_3 rich compositions revealed a specular transmission of ~40–60% in the same wavelength range with a high degree of transparency. Additionally, effect of chemical composition on the fracture toughness of spinel ceramics was investigated applying indentation and chevron notched specimen fracture toughness measurement techniques. The spinel ceramic with $n = 2.0$ revealed the highest fracture toughness with a mean value of ~2.02 $MPa{\cdot}m^{1/2}$. Based on their optical and mechanical properties, potential of Al_2O_3 rich non-stoichiometric polycrystalline spinel ceramics for engineering applications requiring high optical transparency and improved fracture toughness was addressed.

(Received December 27, 2004; Accepted March 11, 2005; Published May 15, 2005)

Keywords: *$MgAl_2O_4$ spinel, optical properties, fracture toughness, microcracking*

1. Introduction

Magnesium aluminate "spinel" ($MgAl_2O_4$) is one of the most outstanding optically transparent ceramics that exhibits a unique combination of optical and mechanical properties both at ambient and elevated temperatures. After being shown to be transparent in early 1960's, spinel has received considerable attention and has been the subject of numerous studies.[1,2,6,8,10–12] It has been considered to be well suited especially for armor applications because of its ideal combination of optical transparency, hardness, impact resistance, strength, modulus, ease of fabrication and crystal size capability.[3–5] In various studies, it has been shown to be superior to other available armor materials such as sapphire, AlON, soda-lime silicate glass and MgF_2 in terms of its excellent balance of performance and affordability.[4,5] Besides being an attractive transparent armor, it is also expected to serve as a high temperature and visible/infrared (IR) window material[6,7] because of its high temperature mechanical properties with chemical inertness to strong acids and alkali solutions[8] as well as its dual optical transparency effective in visible and mid-IR wavelength ranges,[2] respectively.

For its applicability as an optical window material, the optical properties of spinel, which are controlled by various factors such as the nature of the starting materials, applied processing route and conditions as well as the resulting microstructure, should be optimized. In this context, there have been several efforts to correlate the optical properties of spinel to the applied processing conditions such as applied sintering, hot-pressing, hot isostatic pressing or annealing parameters and the resulting microstructural features.[9–13]

However, although magnesium aluminate spinel exists in a wide composition range because of the high solid solubility of Al_2O_3 in MgO[14] that is expressed by the formula $MgO{\cdot}nAl_2O_3$ ($1 \leq n < 3$), the effect of chemical composition on the light transmittance of spinel has not been investigated thoroughly in a wide spectrum range from the visible to the IR wavelengths. The present study has focused on the chemical composition dependence of the optical properties of magnesium aluminate spinel ceramics. Light transmittance of spinel with $n = 1.0$, 1.5 and 2.0 was addressed for the UV/visible/near-IR wavelength ranges and discussed in relation to the resulting microstructures. Furthermore, the effect of the chemical composition on the fracture toughness of spinel ceramics has been investigated to determine the mechanical capacity of non-stoichiometric spinel compositions for various engineering applications demanding high optical transparency along with mechanical reliability.

2. Experimental Procedure

2.1 Materials and fabrication process

Commercially available high purity MgO (purity 99.98 mass%, 1000A, Ube Chemicals Co. Ltd., Ube, Japan) and Al_2O_3 (purity 99.99 mass%, TM-DAR, Taimei Chemicals Co. Ltd., Nagano, Japan) powders having average particle sizes less than 0.12 and 0.15 μm, respectively, were used as the starting materials in this study. The starting ceramic powders were mixed by a mechanical preparation process; the details were reported elsewhere.[13] Al_2O_3 content was changed in the powder mixture in order to obtain three different final compositions of $MgO{\cdot}nAl_2O_3$ with $n = 1.0$, 1.5 and 2.0, which will be denoted as "spinel I," "spinel II" and "spinel III," respectively, hereafter.

*[1]Present Address: National Institute for Materials Science, International Center for Young Scientists, Ibaraki 305-0047, Japan
*[2]Graduate School of Engineering, The University of Tokyo

Mechanically mixed starting materials with three different $MgO:Al_2O_3$ molar ratios were consolidated by a two-stage process of hot-pressing followed by hot isostatic pressing (HIPing). Hot-pressing was performed at 1673 K in vacuum (10^{-2} Pa) for 1 h under a pressure of 50 MPa. The milky white hot-pressed compacts were then hot isostatically pressed (HIPed) at 2173 K in argon for 1 h under a pressure of 189 MPa in order to eliminate residual porosity and obtain optically transparent magnesium aluminate spinel ceramics. After HIPing, compacts were mechanically cut to ~2 and ~4 mm thick blocks, and their surfaces were polished by a standard metallographic process up to 0.5 μm diamond paste finish.

2.2 Structural characterization

Chemical compositions of the fabricated spinel ceramics were determined by inductively coupled plasma spectroscopy within an accuracy ±0.1 mass%. Microstructure of the spinel ceramics was examined using a conventional optical microscope. Fracture surfaces of the mechanically tested samples were also examined by a conventional scanning electron microscope. Crystalline structure of the spinel compacts was determined by X-ray diffraction analysis (XRD) using a conventional X-ray diffractometer (RINT2500, Rigaku Corporation, Tokyo, Japan) with a Cu target. Densities of the samples were measured using Archimedes' principle, at room temperature (297 K) with ethyl alcohol as the immersion medium with an accuracy $\pm 0.003\ g/cm^3$.

2.3 Determination of optical properties

Light transmittance measurements both in the UV/visible and near-IR wavelength ranges were employed to determine the optical properties of the fabricated spinel ceramics. UV/visible light transmittance measurements were conducted in a wavelength range between 250 and 2000 nm using a transmission optical spectrometer (Jasco V-550 type, Nihon Bunko Corp., Tokyo) with a nominal resolution less than 2 nm in this range. Measurements were performed on 2.0 and 4.0 ± 0.02 mm thick specimens at a fully controlled temperature of 297 K. Total transmission and reflection spectra of the spinel ceramics parallel to the hot-pressing direction were obtained by the integrating sphere attachment (ISN-470, Nihon Bunko Corp., Tokyo) of the spectrometer. Additionally, in-line transmission spectra of the spinel ceramics were obtained through a 4 by 4 mm slit attached on the specimen surface that allowed the detection of only the specularly transmitted portion of the incident light beam.

Near-IR transmittance of the spinel ceramics was determined with a Fourier transformation infrared spectrometer (FT/IR-620 Plus, Nihon Bunko Corp., Tokyo) in a wavelength range from 2000 to 25000 nm at 298 K using 4.0 ± 0.02 mm thick specimens. In-line transmission and reflection spectra were obtained in this range. During both the UV/visible and the near-IR transmittance measurements specimens were rotated by 90 degrees after each measurement in order to eliminate the polarization effects, and the average of the four obtained spectra was used for the analysis.

2.4 Fracture toughness measurement

2.4.1 Indentation

Fracture toughness, K_{Ic}, of spinel ceramics was measured by indentation technique on polished surfaces. Different indentation loads were applied: loads of 0.65, 0.80 and 1.0 N by microindentation device on an optical microscope, and loads of 3.0 and 5.0 N by standard Vickers indenter. The lower loads often led to indentation cracks in two corners of indentation mark. The highest loads (3.0 and 5.0 N) led to a large amount of cracking around the indentation, very often up to 6-7 indentation cracks. However, still both the crack length values and their geometry were acceptable for the application of the following equation because of its suitability for this type of materials:[15]

$$K_{Ic} = 0.016(E/H)^{1/2}F/c^{3/2}. \quad (1)$$

The value c in this equation represents half of penny shaped radial crack measured on the indented specimen surface where F and H are the applied load and the hardness of the ceramic, respectively. As Young's modulus, E, the value 259 GPa was used, which is the mean value of the Young's modulus range of 248–270 GPa reported for stoichiometric $MgAl_2O_4$ in the literature.[6] During this test, indentation cracks were evaluated separately for each indention to calculate the fracture toughness.

2.4.2 Three point bending with chevron notched specimen

Critical applied stress intensity factor of the spinel ceramics was determined by the chevron notched (CN) specimen technique. The geometry employed is schematically illustrated in Fig. 1. Chevron notches with an angle of 90° were inserted using a thin diamond cutter. The specimens were loaded in three-point bending (span of 16 mm) at a constant cross-head speed of 0.01 mm/min. The tests were carried out at room temperature in ambient atmosphere. Since the span of the three-point bend test was 16 mm, it was possible to introduce two notches in each bar, *i.e.* two fracture toughness tests were carried out using each bar. This approach, single test bar with two notches keeping the same loading geometry, enables to carry out more tests than in the

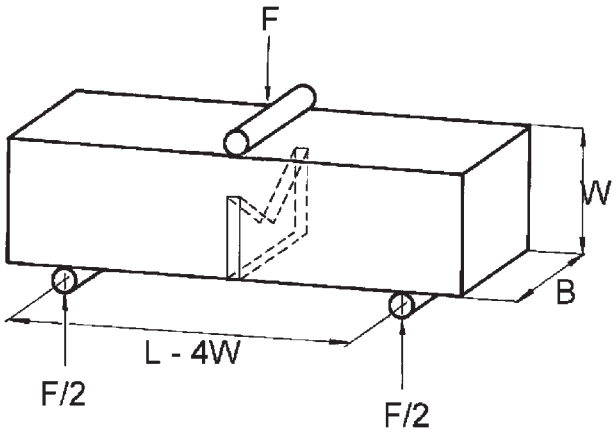

Fig. 1 Schematic of the chevron notched specimen geometry employed for toughness determination of spinel ceramics.

Table 1 Measured composition, density and amount of microcracking of fabricated spinel ceramics.

Sample	$MgO:Al_2O_3$ Molar Ratio	mass% Mg	mass% Al	Percent of Theoretical Density (%)	Grain Boundary Microcracking, S_v^{Mc} (mm^{-1})
Spinel I	1:1	16.9	38.1	99.86	1.30
Spinel II	1:1.5	12.3	41.8	99.92	0.41
Spinel III	1:2	9.90	44.1	99.78	0.57

case of separate short samples. Each bar with notches was placed in the three-point bending fixture and loaded up to fracture initiation. After each test the bar was moved to place the other chevron notch into position in the three point bending rig.

Graphs of load versus deflection were recorded and the critical applied stress intensity factor, $K_\infty{}^c$, was calculated from the fracture load (F_{max}) and the corresponding minimum value of the geometrical compliance function ($Y^*{}_{min}$) using the equation:[16)]

$$K_\infty{}^c = F_{max} Y^*{}_{min}/BW^{1/2} \quad (2)$$

where B and W are the width and height of the specimens, respectively. The calculation of the function $Y^*{}_{min}$ for chevron notched bending bars was based on Bluhm's slice model.[17)] The chevron-notch depth, a_o, was measured from optical macrographs of the fractured specimens.

3. Results and Discussion

3.1 General characteristics

The results of the inductively coupled plasma spectroscopy confirmed the chemical composition of the spinel ceramics exactly matching to the intended relative molar ratios of MgO and Al_2O_3 by controlling the amounts of starting materials (Table 1). X-ray diffraction analysis of the fabricated spinel ceramics revealed the presence of magnesium aluminate spinel as the single phase for all of three compositions. Although a slight shift in the peak positions was observed in the XRD patterns of spinel II and spinel III samples compared to that of the reference data[18)] because of the non-stoichiometry in their compositions, there is a close match between them. Applied processing route composed of hot-pressing followed by HIPing has led to highly dense spinel ceramics with final relative densities ranging from 99.78 to 99.92% (Table 1) of the theoretical density of $MgAl_2O_4$ ($\rho_{theo} = 3.58\,g/cm^3$).[10)] As the main cause of attenuation of light transmission through a ceramic body is scattering by residual porosity,[19,20)] near-full densification is the highest priority requirement to obtain optical transparency in ceramic materials.

All of the spinel ceramics obtained in the present study revealed a considerable degree of optical transparency independent of the chemical composition. Figure 2 shows fabricated spinel ceramics which are placed on a piece of written paper where the underlying image is visible through all of them. As the samples were not heat treated after fabrication, spinel II and spinel III seem to be slightly darker in color because of carbon contamination from the hot-pressing die during processing. However, despite this coloring effect they reveal a comparable visible clarity to that of spinel I.

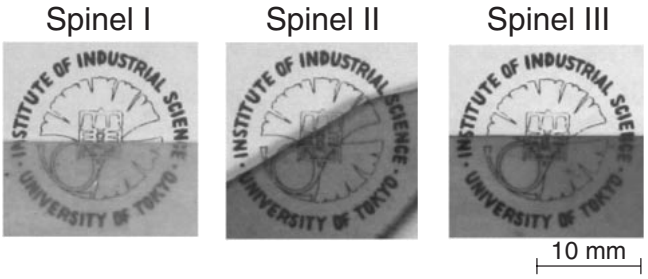

Fig. 2 Macroscopic appearance of the fabricated transparent spinel ceramics.

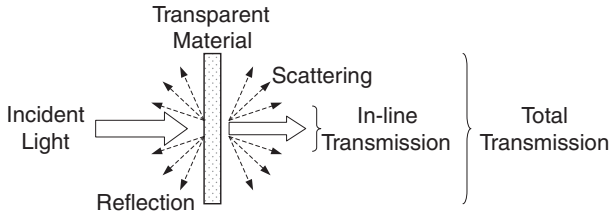

Fig. 3 Schematic illustration of the interaction of light with an optically transparent material explaining the terminology referred throughout the text.

3.2 Optical properties

In the scope of the present discussion, optical properties of the fabricated spinel ceramics is addressed by correlating their total and in-line transmittance as well as their reflectance to their microstructure and resulting optical transparency. The interaction of light with an optically transparent material is illustrated in Fig. 3. When a beam of light is incident to a material, it reflects at the external and also internal surfaces, attenuates in the interior of the material, and the rest of it transmits through the material both specularly and diffusely. The ratio of the intensities of the reflected and attenuated light to that of the incident beam is termed as reflectance, R, and attenuation, A, respectively. The total amount of light emerging from the material is termed as total transmittance, T, while its specularly transmitted portion is termed as in-line transmittance, T_{in}, after taking scattering into account as a possible loss mechanism in the transmission process. As a consequence of conservation of energy the following relation holds between the above mentioned portions of light involved in each process for a given wavelength, λ:

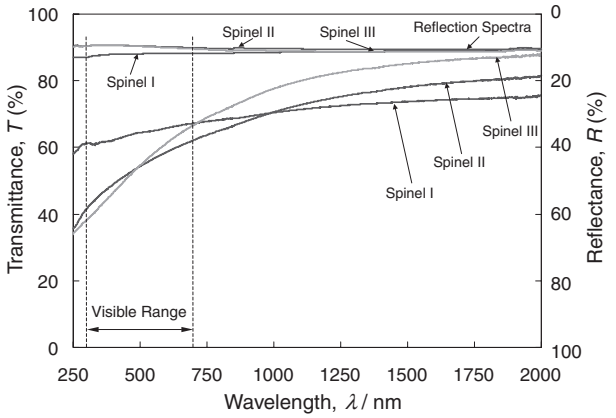

Fig. 4 Reflection and total transmission spectra of the fabricated spinel ceramics in the UV/visible wavelength range measured using ∼2 mm thick specimens.

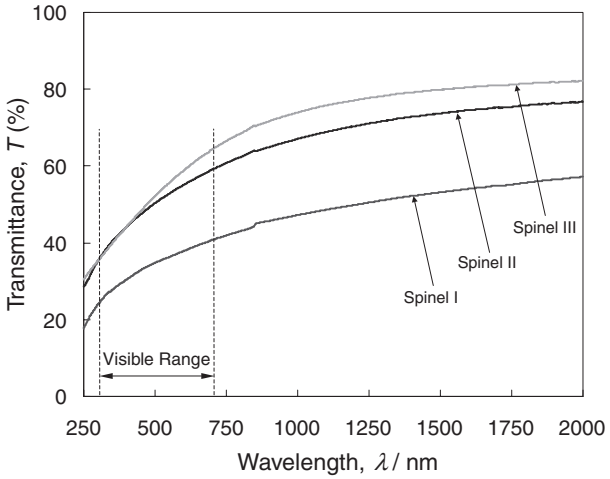

Fig. 5 In-line transmission spectra of the fabricated spinel ceramics in the UV/visible wavelength range measured using ∼2 mm thick specimens.

$$R + A + T_{\text{in}} = 1. \tag{3}$$

Figure 4 demonstrates the total transmission and reflection spectra of the fabricated spinel ceramics. Reflection spectra of spinel II and spinel III are nearly constant at a value of ∼10% throughout the measured wavelength range. On the other hand, although the reflectance of spinel I is nearly equal to those of the other samples at higher wavelengths, it increases to ∼14% in the visible wavelength range. This implies the presence of a larger amount of internal surfaces in spinel I, as the external surfaces of all of the samples were brought to the same surface finish by an identical process. Unlike their reflectance, total transmittance of the spinel ceramics shows stronger wavelength dependence revealing a variety of values in different wavelength ranges. However, for all of the samples total transmittance decreases by decreasing wavelength because of absorption losses.[21] In the measured wavelength range the total transmission spectra of spinel III changes between ∼35% and ∼87% being the highest of all above 1000 nm, while spinel I has a total transmission spectrum that changes between ∼60 and 78% in the same wavelength range that reveals the highest values in the visible range.

Although there is not a well-defined direct correlation between the light transmittance and optical transparency of a material, specularly transmitted portion of light has a stronger effect on the resulting visible transparency. In-line transmission spectra of the fabricated spinel ceramics are shown in Fig. 5. The in-line transmission spectra of spinel II and spinel III show a similar trend as in the case of their total transmission, where spinel III has slightly higher transmittance values throughout the measured wavelength range. On the other hand, spinel I reveals an in-line transmission spectrum that changes between ∼20 and 57% between 250 and 2000 nm being 10 to 20% lower compared those of the other samples in the visible wavelength range.

In-line transmittance of the spinel samples measured in the near-IR wavelength range shows a similar trend to that observed in the UV/visible range (Fig. 6), although they are lower in average due thicker specimens (∼4 mm) used for the measurements. In the near-IR range spinel III revealed the highest in-line transmittance of ∼70% between ∼2000 and 4500 nm while spinel I revealed the lowest in-line transmittance of ∼30% in the same wavelength range. The peaks observed for all of the three spectra at ∼4250 nm is caused by the continuous change of the CO_2 present in the measurement atmosphere (ambient air) that did not allow accurate background corrections.[22] In the case of spinel III, an absorption band is observed at ∼3000 nm, which is most probably due to the entrapped water in the ceramic,[23] that is not seen in the near-IR in-line transmission spectra of spinel I and II samples.

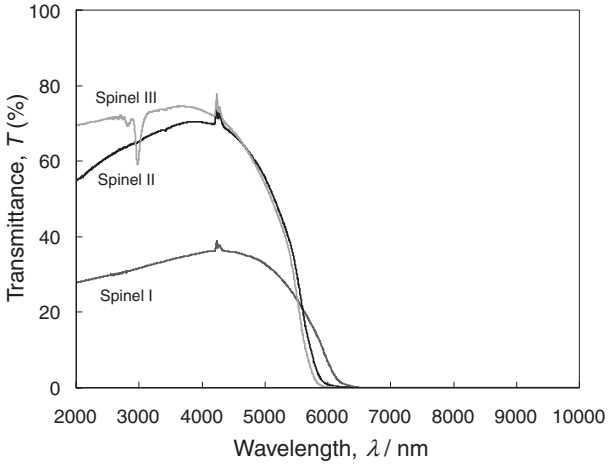

Fig. 6 In-line transmission spectra of the fabricated spinel ceramics in the near-IR wavelength range measured using ∼4 mm thick specimens.

3.3 Quantitative analysis of light transmission behavior

In order to understand the contribution of different factors resulting in the observed transmittance behavior of the spinel ceramics, reflection and total and in-line transmission spectra of spinel I is examined on a single graph as a representative example (Fig. 7). The region remaining above the reflection spectrum corresponds to the reflection losses that occurred at the external and internal surfaces of the spinel ceramic. The dotted area between the reflection and total transmission

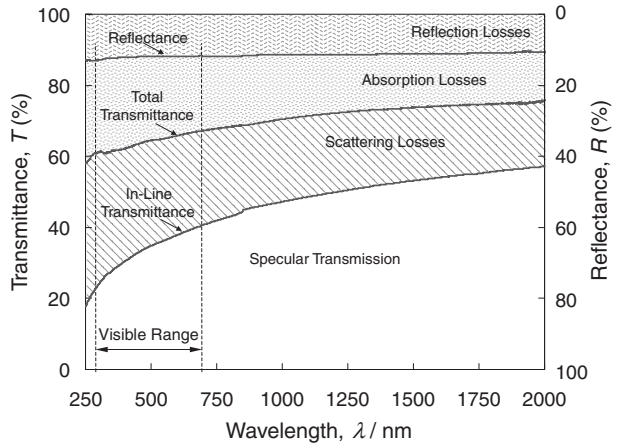

Fig. 7 Reflection and total and in-line transmission spectra of spinel I in the UV/visible wavelength range showing the reflection, absorption and scattering losses.

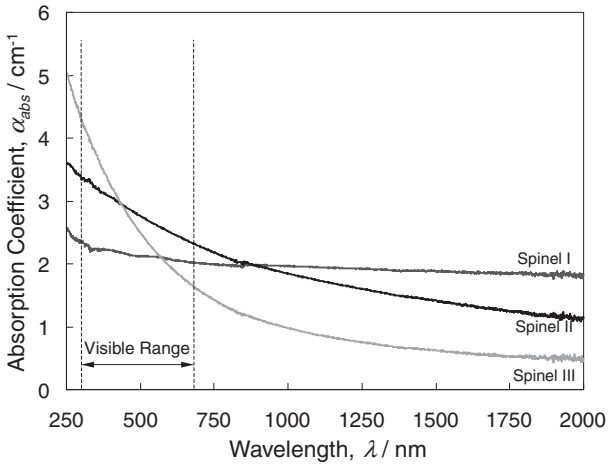

Fig. 8 Change of absorption coefficient of fabricated spinel ceramics with wavelength.

spectra shows the amount of absorption losses that most probably resulted from the impurities in the material the presence of which was reported by the present authors for spinel ceramics fabricated with the same processing route.[13] In addition to this, multiple scattering losses, if there are any, were also included in the absorption losses, which is the portion of the emerging beam that could not be captured by the integrating sphere attachment of the spectrometer during the total transmittance measurement. The striped region between the total and in-line transmission spectra corresponds to the scattering losses in the spinel ceramic. The rest of the graph remaining below the in-line transmission spectrum corresponds to the amount of the specularly transmitted light through the spinel ceramic that mostly accounts for the resulting optical transparency. Absorption and scattering losses shown in Fig. 7 constitutes the two sources of the total attenuation in the spinel ceramics, which are quantified as the absorption and scattering coefficients, respectively, using the measured reflectance and transmittance values.

The in-line transmittance, T_{in}, of a material is given by

$$T_{\text{in}} = (1 - R)^2 \exp(-\alpha t) \tag{4}$$

in terms of its reflectance, R, attenuation coefficient, α, and thickness, t, where the attenuation coefficient is composed of the absorption, α_{abs}, and scattering α_{sca}, coefficients. As a result of this, in-line transmittance of a material is expressed by

$$T_{\text{in}} = (1 - R)^2 \exp[-(\alpha_{\text{abs}} + \alpha_{\text{sca}})t] \tag{5}$$

while its total transmittance is given by

$$T = (1 - R)^2 \exp(-\alpha_{\text{abs}} t) \tag{6}$$

as it contains absorption as the only loss mechanism. Having measured the total and in-line transmission spectra of the spinel ceramics for two different specimen thicknesses, their absorption and scattering coefficients are obtained by a simple mathematical treatment rearranging eqs. (5) and (6).

With this treatment a quantitative comparison of the absorption and scattering behaviors of the fabricated spinel ceramics is done relative to each other using their transmittance and reflectance properties that were determined under identical conditions. Figure 8 shows the absorption coefficients of the spinel ceramics as a function of wavelength. The absorption coefficients decrease towards higher wavelengths where impurity atoms have less electronic transitions.[24] The difference of the processing related impurity content of the present spinel ceramics,[13] however, gives rise to variations in their absorption coefficients in different spectral ranges. In the visible wavelength range, spinel III has the highest absorption coefficient at lower wavelengths, while at higher wavelengths spinel I and II show higher absorption, where the observed differences range between $\sim$0.7 and 2 cm^{-1}.

Wavelength dependence of the scattering coefficients of the spinel ceramics is shown in Fig. 9. The scattering coefficients decrease with increasing wavelength implying that the size of the scattering centers present in the spinel ceramics mostly correspond to the lower wavelength side of the measured spectrum, since scattering in the forward direction increases as the size of the scattering centers approaches to the wavelength of the incident light.[25] Unlike

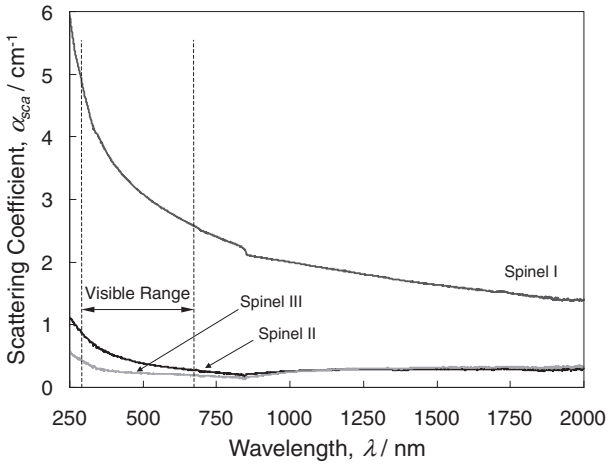

Fig. 9 Wavelength dependence of the scattering coefficient of fabricated spinel ceramics.

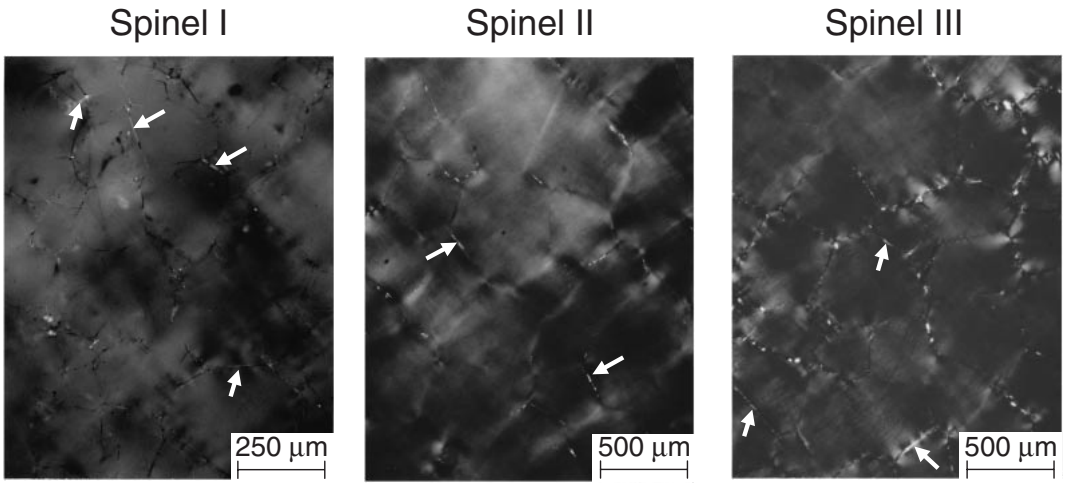

Fig. 10 Microstructure of the polished section of fabricated spinel ceramics under cross-polarized transmission light showing microcracking along grain boundaries.

the case with the absorption coefficients, the scattering coefficient of spinel I is distinctly higher from those of spinel II and III throughout the measured spectrum, which range between ~0.5 and 1 cm^{-1}. In the visible wavelength range, the scattering coefficient of spinel I ranges between ~2.6 and 4.8 cm^{-1} that is nearly 5–10 times higher then the scattering coefficients of spinel II and III in the same range. This implies the presence of a higher amount of scattering cites in spinel I compared to the other samples.

3.4 Grain boundary microcracking and optical transparency relation

The sources of light scattering in transparent ceramics are residual porosity, second phases and grain boundaries.[21] As the amount of residual porosity is nearly the same and negligible in all of the fabricated spinel ceramics, which are composed of a single magnesium aluminate spinel phase, scattering losses should somewhat be related to the grain boundaries. Examination of the spinel ceramics under cross-polarized transmission light by an optical microscope revealed the presence of grain boundary microcracking in all samples (Fig. 10). Although the presence of microcracking is unexpected in cubic crystals like spinel due to their isotropic properties, similar instances were also reported for zirconia and spinel ceramics.[13,26]

The amount of grain boundary microcracking present in the spinel ceramics was quantified as the microcracked grain boundary surface area per unit volume, S_v^{Mc}, using a stereological relationship[27,28] defined by

$$S_v^{Mc} = 2P_L^{Mc} \tag{7}$$

where P_L^{Mc} is the density of the intersection points of the microcracked grain boundaries with the test lines drawn on the micrographs shown in Fig. 10. Spinel I reveals the highest amount of microcracking that is ~2 to 3 fold those of the spinel II and III samples (Table 1). The magnification of the micrograph shown in Fig. 10(a) is two times that of the other two micrographs, and therefore, yields the highset value for S_v^{Mc}, although microcracking content seems to be lower. This result is consistent with the higher scattering coefficient of spinel I shown in Fig. 9.

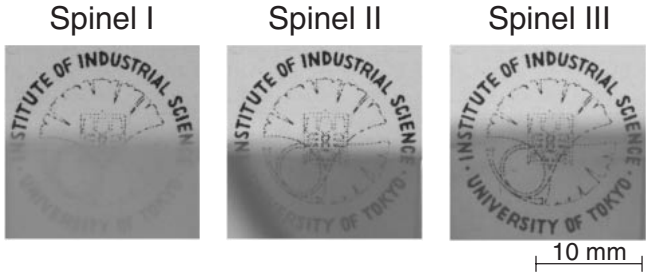

Fig. 11 Appearance of the underlying object through the spinel ceramics that are placed ~5 cm above the plane of the image.

Figure 11 shows the effect of scattering on the optical transparency of the fabricated spinel ceramics. In these photographs, unlike the case shown in Fig. 2 the samples are placed ~5 cm above the plane of the underlying image. As can be seen from the figure, although spinel II and III ceramics still reveal a high degree of visible clarity, the underlying image is hardly visible through spinel I. This shows the effect of pronounced scattering because of the relatively higher microcracking content of spinel I that makes it difficult to resolve the image against the scattered background compared to the other spinel ceramics.

3.5 Fracture toughness of spinel ceramics

The indentation fracture toughness values of the spinel ceramics and their standard deviations are summarized in Table 2. Each value represents the mean value from at least 5 indentations. All measurements have high experimental scatter. Hardness values having standard deviations up to ~200 HV is provided as an indication of the scatter. Similarly, observed indentation cracks have evident differences both in length and morphology, which is related to the scattering in grain size distribution of the present spinel ceramics depicted on the fracture surface of spinel I (Fig. 12). Despite the scatter in the measured data, spinel III reveals the highest fracture toughness values ranging between 1.65 and 2.21 $MPa \cdot m^{1/2}$.

Table 2 Indentation toughness, K_{Ic}, values of fabricated spinel ceramics along with their Vickers hardness (HV), average of five measurements.

Indentation Load (N)	Spinel I			Spinel II			Spinel III		
	HV	*c* (μm)	K_{Ic} (MPa·m$^{1/2}$)	*HV*	*c* (μm)	K_{Ic} (MPa·m$^{1/2}$)	*HV*	*c* (μm)	K_{Ic} (MPa·m$^{1/2}$)
0.65 (μ)	1499	20.5	1.47 ± 0.16	1778	22.3	1.19 ± 0.15	1528	25.9	1.65 ± 0.17
0.80 (μ)	1523	22.5	1.56 ± 0.15	1711	28.9	1.18 ± 0.11	1566	20.6	1.76 ± 0.12
1.00 (μ)	1603	24.5	1.67 ± 0.13	1698	28.8	1.28 ± 0.09	1418	23.5	1.90 ± 0.11
3.00	1857	46.5	1.79 ± 0.28	1259	64.1	1.34 ± 0.21	1853	40.4	2.21 ± 0.21
5.00	1618	71.1	1.69 ± 0.21	1368	91.1	1.27 ± 0.19	1725	61.9	2.01 ± 0.19

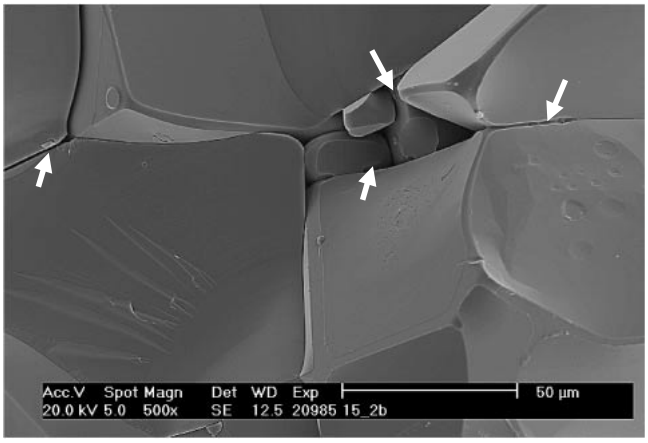

Fig. 12 Fracture surface of spinel I after testing a chevron notched specimen where grain boundary microcracking and non-uniformity of the microstructure are indicated by arrows.

Table 3 Critical applied stress intensity factor values of spinel III obtained by chevron notched three-point bend specimens.

Measurement	*W* (mm)	*B* (mm)	F_{max} (N)	a_o (mm)	$K_{\infty}{}^{c}$ (MPa·m$^{1/2}$)
1	4.18	2.02	22.76	1.45	1.84
2	4.08	2.02	20.60	1.66	2.17
3	5.05	2.01	30.12	2.12	2.19
4	4.97	2.01	31.18	2.05	2.27
5	4.09	2.01	20.76	1.45	1.83
6	3.92	2.00	17.18	1.49	1.80

The raw data obtained by testing the chevron notched specimen of spinel III is given in Table 3 as a representative one. The mean fracture toughness of spinel III is 2.02 MPa·m$^{1/2}$, which is the highest value of all spinel ceramics measured with this method. When the experimental results obtained by the two methods are compared indentation toughness values seem to be consistently lower for all of the spinel compositions. This is related to the measured indentation crack sizes being smaller than the average grain sizes of the present spinel ceramics, which are above 100 μm (Fig. 10). As a result of this, the indentation cracks are mostly confined in a single grain giving in a sense the fracture toughness of a single spinel crystal. In addition to that the absence of stress relief treatment after polishing the samples gives rise to the presence of residual stresses in the materials contributing to indentation crack formation and lowering the indentation toughness values. Moreover, the experimental error of the microcrack length determination may have also affected the final indentation fracture toughness values. In the case of the chevron notched specimens, however, advancing crack interacts with the microstructures in the spinel ceramics associated with energy dissipation resulting in higher applied stress intensities to be measured. Nevertheless, fracture toughness determination by three point bending with chevron notched specimen revealed more consistent results with lower experimental scatter compared to indentation method.

In the present discussion, the issue of correlating the observed fracture toughness values of the fabricated spinel ceramics to their microstructural features could be rather complex. This point arises from the fact that the two applied fracture toughness testing methods namely the indentation and chevron notched three-point bend bar involve microflaws and macro-notches as their artificial stress concentrators, respectively, which interact with the microstructures of the material differently leading to the difference in the resulting process zone and crack wake. In this respect, crack face tractions operating in the wake typical of coarse grain sized spinels[29] should be considered for the chevron notched specimen. On the other hand, in the case of the indentation method the shielding effect of the grain boundary microcracks on the measured fracture toughness of the fabricated spinel ceramics can be argued. Eventually, in the present study although a direct correlation could not be established between the microstructural features and the fracture toughness of the spinel ceramics based on two different measurement methods, consistency of the two methods was confirmed by the highest fracture toughness of spinel III determined using these methods.

Light transmittance of the spinel ceramics obtained in the present study are comparable with that of the stoichiometric hot-press/HIPed spinel ceramics fabricated from high purity spinel powders that reveal ~50–85% transmission in the wavelength range between 250 and 2000 nm.[10] However, the visible range transmission of the present spinel ceramics are slightly lower compared to the reported data because of the impurity absorption, which is a consequence of the used raw materials and the applied processing route. Even though this is the case, visible range absorption coefficients of the present spinel ceramics are either similar or lower compared to those of the spinel ceramics of another study that were fabricated by HIPing at a lower temperature and pressure.[4] Reported absorption coefficient of 2.5 cm^{-1} at a wavelength of 700 nm

is similar to that of spinel II of the present study, while spinel I and III ceramics reveal lower absorption coefficients at the same wavelength.

In addition to their optical properties comparable to spinel ceramics obtained from high quality spinel powders reported in the literature, fracture toughness of the present non-stoichiometric spinel ceramics revealed an improvement over the fracture toughness values reported for stoichiometric spinels. The mean fracture toughness of spinel III ceramic of the present study is superior to that of a pure stoichiometric spinel reported in another study fabricated by a rate-controlled sintering and HIPing route[8] that revealed a fracture toughness of 1.7 $MPa \cdot m^{1/2}$. Consequently, present study showed that besides the stoichiometric $MgAl_2O_4$ spinel ceramics, Al_2O_3 rich non-stoichiometric spinel compositions should also be considered as potential materials for engineering applications in terms of their high light transmittance and considerable optical transparency along with improved fracture toughness.

4. Concluding Remarks

Transparent magnesium aluminate "spinel" ceramics were fabricated using hot-pressing and hot isostatic pressing (HIPing). Al_2O_3 content of the starting powder mixture was changed to obtain spinel ceramics with three different final compositions, $MgO \cdot nAl_2O_3$, where $n = 1.0$, 1.5 and 2.0. Optical properties of spinel ceramics were quantitatively discussed in relation to their microstructure. Presence of microcracking at the grain boundaries of the spinel ceramics that causes excessive light scattering losses was evidenced by optical microscopy observations. The spinel ceramic with a MgO to Al_2O_3 molar ratio of 1:1 revealed the highest scattering coefficient with its highest amount of grain boundary microcracking making it difficult to resolve images through this sample. Chemical composition was also found to affect the fracture toughness of spinel ceramics, as measured by indentation and three point bending with chevron notched specimen. The spinel ceramic with $n = 2$ revealed the highest fracture toughness with a mean value of $\sim$2.02 $MPa \cdot m^{1/2}$, as determined by chevron notched specimen technique. The optical properties of non-stoichiometric spinel ceramics are comparable with literature data while their fracture toughness is higher compared to published results on stoichiometric spinel ceramics.

Acknowledgement

ARB acknowledges the financial support of the Royal Society (London, UK).

A part of the present research was financially supported by grant Nr. A2041003 of the Grant Agency of the Academy of Sciences.

The authors gratefully acknowledge M. Yamamoto for the preparation of the spinel ceramics and Z. Chlup for carrying out SEM investigations.

REFERENCES

1) R. J. Bratton: J. Am. Ceram. Soc. **57** (1974) 283–286.
2) M. C. L. Patterson, J. E. Caiazza and D. W. Roy: Proc. SPIE **4102** (2000) 59–68.
3) G. Gilde, P. Patel and M. Patterson: Proc. SPIE **3705** (1999) 94–104.
4) D. W. Roy and G. G. Martin, Jr.: Proc. SPIE **1760** (1992) 2–13.
5) J. J. Swab, J. C. LaSalvia, G. A. Gilde, P. J. Patel and M. J. Motyka: Ceram. Eng. Sci. Proc. **20** (1999) 79–84.
6) D. W. Roy and J. L. Hastert: Ceram. Eng. Sci. Proc. **4** (1983) 502–509.
7) D. S. Tsai, C. T. Wang, S. J. Yang and S. E. Hsu: Mater. Manuf. Processes **9** (1994) 709–719.
8) K. E. Green, J. L. Hastert and D. W. Roy: Proc. SPIE **1112** (1989) 2–8.
9) M. Shimada, T. Endo, T. Saito and T. Sato: Mater. Lett. **28** (1996) 413–415.
10) D. W. Roy: Proc. SPIE **297** (1981) 13–18.
11) K. Hamano and S. Kanzaki: Yogyo-Kyokai-Shi **85** (1977) 225–230.
12) S. Kanzaki, K. Saito, Z. Nakagawa and K. Hamano: Yogyo-Kyokai-Shi **86** (1978) 485–491.
13) A. F. Dericioglu and Y. Kagawa: J. Eur. Ceram. Soc. **23** (2003) 951–959.
14) E. M. Levin and H. F. McMurdie: *Phase Diagrams for Ceramists 1975 Supplement*, (The American Ceramic Society Inc., Ohio, 1975) pp. 114, 135.
15) G. R. Anstis, P. Chantikul, B. R. Lawn and D. B. Marshall: J. Am. Ceram. Soc. **64** (1981) 533–538.
16) A. R. Boccaccini, R. D. Rawlings and I. Dlouhy: Mater. Sci. Eng. **A 347** (2003) 102–108.
17) J. I. Bluhm: Eng. Fract. Mech. **7** (1975) 593–604.
18) National Bureau Standards (U.S.) Monogr. **25** (1971) 9–25.
19) M. Erneta and H. A. Stockler: J. Am. Ceram. Soc. **56** (1973) 394–395.
20) J. G. J. Peelen and R. Metselaar: J. Appl. Phys. **45** (1974) 216–220.
21) M. Baas (Editor in Chief): *Handbook of Optics v. II*, (McGraw-Hill Inc., New York, 1995) p. 33.19.
22) W. L. Wolfe and G. J. Zissis: *The Infrared Handbook*, (ONR, Department of Navy, Washington, 1978) p. 5–70.
23) W. G. Driscoll and W. Vanghan: *Handbook of Optics*, (McGraw-Hill Inc., New York, 1978) p. 7.52.
24) E. Hecht: *Optics*, (Addison-Wesley Publishing Company Inc., New York, 2002) p. 67.
25) J. Schroeder and J. H. Rosolowski: Proc. SPIE **297** (1981) 156–168.
26) K. Ahlborn, Y. Kagawa and A. Okura: Fracture Mech. Ceram. **10** (1992) 47–58.
27) K. J. Kurzydlowski and B. Ralph: *The Quantitative Description of the Microstructure of Materials*, (CRC Press Inc., Boca Raton, 1995) p. 20.
28) K. J. Kurzydlowski and B. Ralph: *The Quantitative Description of the Microstructure of Materials*, (CRC Press Inc., Boca Raton, 1995) p. 275.
29) J. C. Hay and K. W. White: *Fracture Mechanics of Ceramics*, ed. by R. C. Bradt *et al.*, (Plenum Press, New York, 1992) p. 265.